Peak Brightness Maximization Through Initial Current Profile Preparation at the Advanced Superconducting Test Accelerator (ASTA)

William Wortley*, Fermilab Lee Teng Intern, IL and the University of Rochester, NY
Jayakar Charles Thangaraj, Fermilab, IL

INTRODUCTION

Both linear colliders and free electron lasers (FELs) require an electron beam of high quality which is determined by certain figures of merit. Two of the most important of these are the emittance and the peak current which together determine the brightness of a beam. The ability to attain a high peak current is closely tied to the ability to longitudinally compress an electron bunch. At ASTA (the Advanced Superconducting Test Accelerator) and many other linear accelerators worldwide, this compression is accomplished with the use of a four-dipole magnetic bunch compressor. The compression results in a beam with a greater longitudinal density and higher peak current which leads to a reduced gain length and thus an increase in radiated power of an FEL. However, due to the bending of the electrons in the dipole magnets, coherent synchrotron radiation (CSR) is emitted which causes an emittance growth in the bending plane (horizontal). With brightness being the ultimate indicator of an accelerator or laser source's performance, the suppression of this horizontal emittance growth, which is inversely proportional to the brightness, is an area of great interest in accelerator physics. In a recent paper, Chad Mitchell proposed a technique for mitigating the effects of CSR on the horizontal emittance growth and energy spread through the preparation of the initial current profile of the beam [1]. We have simulated tests of an assortment of different initial current profiles which were then run through the ASTA beamline to determine if certain initial profiles could result in a higher final brightness. We speak first of the background behind the compression process followed by the manner of our testing and bunch generation, and then finally we present our findings.

RF ACCELERATION AND COMPRESSION

In a linear accelerator, longitudinal compression of an electron bunch is often desired. To accomplish this, a (near) linear momentum chirp is imparted to the beam through radiofrequency cavities. As their name suggests, these cavities have an oscillating, sinusoidal electric field and thus voltage across them. By synching the arrival of an electron bunch with the voltage oscillations, it is possible to impart different energies along the bunch.

Here it should be noted that the average quantities of the bunch are often referred to as the qualities of the 'reference particle'. Regardless of whether or not such a particle actually exists in an accelerator, many quantities including distances and energies are given in relation to the reference particle which follows a perfect/idealized trajectory through the accelerator.

Because of the finite length of the bunch, the head and tail of the bunch "see" different voltages. Typically the head of the bunch which arrives first, encounters a lower voltage and gains less energy than the tail of the bunch which arrives later and gains more energy due to the rising rf-waveform (Figure 1). A chirp (often abbreviated as h) is an energy difference per distance $\frac{d\delta}{dz}$ where δ is the energy spread of the bunch, and z is the longitudinal distance along the direction of propagation of the beam. The energy spread of the bunch, δ, itself is the the change in energy across the length of the bunch relative to the average energy of the bunch $\frac{\Delta E}{E}$.

With a carefully prepared chirp, the bunch then enters the four-dipole magnetic chicane. The chicane consists of four dipole bending magnets that are used to bend the electron bunch away from and then back onto its previous trajectory. The Larmor radius formula; $\rho = \frac{p}{eB}$ where p is the momentum of a particle, e is the charge on an electron, and B is the magnitude of the magnetic field strength; which describes how a charged particle bends in the presence of a magnetic field, shows that the bending radius is proportional to the momentum of the particle. After the formula has been rearranged slightly using the knowledge that our electrons are ultrarelativistic ($E_{total} \approx E_{kinetic}$) and that the bending radius is inversely related to the bending angle by a factor of the trajectory length in the dipole l, it reads as such: $\theta_{bend} \approx \frac{leBc}{E}$ with c being the speed of light. Clearly particles with more energy will be bent less than particles with less energy. Because of this bending angle difference, the total path length traversed by individual particles through the chicane becomes energy dependent with the higher energy particles in the tail of the bunch traveling less distance and thus catching up to the lower energy particles in the head of the bunch. Figure 2 shows this difference in energy spread across the bunch. It is important to note that here and throughout the rest of this paper, the head of the bunch will be at negative values of z. The stages of compression through the chicane are illustrated nicely in Figure 3 which shows the time-compression of the phase-space ellipse as well as the time profile.

* wwortley@u.rochester.edu

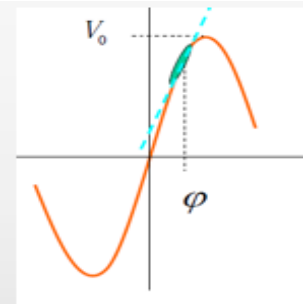

Figure 1: Rf-voltage plotted as a function of z with the bunch positioned to receive an energy chirp.

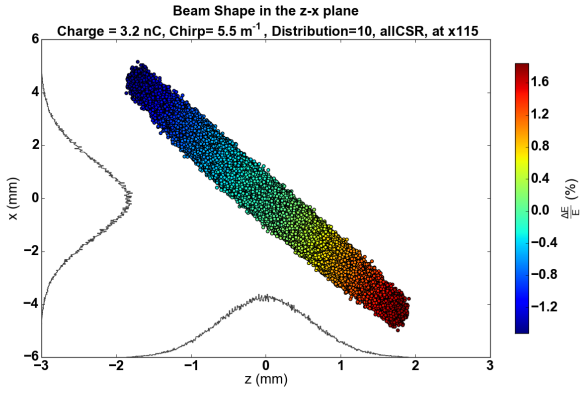

Figure 2: Two dimensional Gaussian beam in the z-x plane with coloring according to energy spread and the corresponding time (z) and horizontal position (x) profiles. Plotted between the second and third dipole magnets (D2 and D3)

EXPERIMENTAL SETUP

In order to model and simulate the ASTA beamline, we used Michael Borland's accelerator simulation code $ELEGANT$ with a beamline created from the ASTA parameters shown in Table 1 [2]. The "lattice" that the simulated electron bunches were run through is shown in Figure 4 and is primarily made up of the first bunch compressor. Due to the large number of simulations being run and the number of initial bunch parameters we wished to be able control, a separate python code was developed to run $ELEGANT$ given any initial set of parameters (chirp, charge, distribution number, initial energy spread, initial bunch length, etc...). The python code also allows for different values of chirp, charge, distribution, and initial bunch length to be looped over. In this way, we were able to set up simulations runs, begin them, and let them run through automatically with no extra supervision. The data relevant to our investigations were saved by the python code into separate and conveniently labeled data files which were then used and analyzed later. To run the data analysis, another python script was written which has the capability to create the large variety of different plots required to visualize and analyze our data. Some of the data extraction

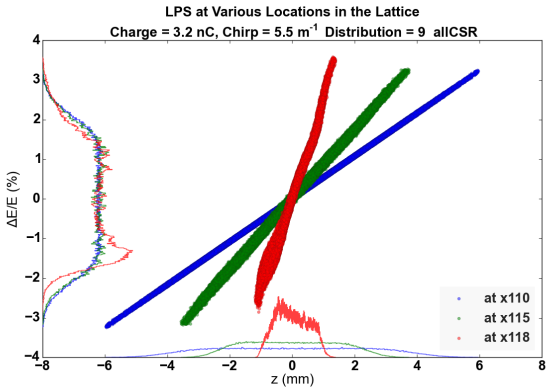

Figure 3: Longitudinal Phase Space with time and energy profiles plotted before D1 (x110) in blue, between D2 and D3 (x115) in green, and after D4 (x118) in red

and analysis was done using $sddstools$ in conjunction with $ELEGANT$. All data, plots, and tables in this paper come from these two python codes.

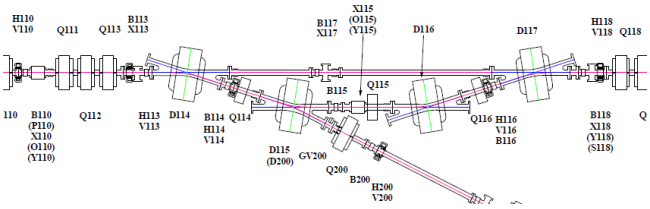

Figure 4: ASTA beamline from watchstation x110 through the first bunch compressor and up to watchstation x118. D114, D115, D116, and D117,are referred to in this paper as D1, D2, D3, and D4 respectively.

INITIAL CHARGE DISTRIBUTIONS

Distribution Generation

All but one of the initial charge distributions [1] we tested were created using a sum of one to four Gaussian functions with different centroid values and amplitudes. In practice we can use lasers in combination with three or more crystals to achieve these profiles [3]. The relative values of the offset (centroid value) and the amplitude were determined and plotted using $Mathematica$. Each of these profiles was then inserted into the python run file. In order to generate them using $ELEGANT$, a file was created that generates each of the single Gaussian bunches from specifications in the run file. The python run file creates each distribution calling the bunch generation file, combines them using the $sddscombine$ command, scales them according to

[1] *The terms 'charge distribution', 'time distribution', 'time profile', 'current profile' and simply 'distribution' will be used interchangeably to refer to the histogram of the time position of all particles relative to the reference particle.

the desired specifications such as number of particles and total bunch length (FWHM), and then runs them through the virtual ASTA lattice. Dist. 18 was generated differently from the others by directly using $sddstools$ and the equation $F[z] = A\frac{(z-a)^{1/3}}{(b-a)^{4/3}}$ where he constants a, b, and A were determined such that the profile would match the other distributions in amplitude and bunch length.

The Distributions

Each distribution is shown in Figures 5 - 13 with an initial full-with-half-max of 2.34 mm which was chosen because it gave the Gaussian profile a sigma of 1 mm. Displayed on each plot is the normalized rms bunch length σ_z [2] and the peak current I_{pk}. Table 2 shows the values of the summed Gaussian functions $\sum_{i=1}^{N} a_i e^{-\frac{(x-b_i)^2}{2}}$ for each distribution.

Table 2: Parameters of Simulation Set Up

Parameter/Element	Value	Unit
Bend Magnet Length	0.301	m
Bending Angle	0.314	rad
Entrance Edge Angle 1 (D2,D4)	0.314	rad
Exit Edge Angle 2 (D1,D3)	0.314	rad
Half-Gap Between Poles	0.025	m
Bins	1000	
Drift Length (D1-D2,D3-D4)	0.5	m
Drift Length (D2-D3)	0.574	m
Number of Kicks (Dipoles and Drifts)	100	
USE_STUPAKOV	1	
Momentum Compaction Factor (R_{56})	0.18	m
Beam Energy	50	MeV
Number of Particles	300	K
Initial Horizontal Emittance	4	μm
Initial Vertical Emittance	4	μm
Initial RMS Energy Spread	2e-04	

SEARCH FOR A FLAT ENERGY PROFILE

Tying into emittance growth minimization was the search for an initial current profile that would result in a flat energy profile of the bunch at the end of the bunch compressor. Intuitively this would be a profile that was similar to a flat top distribution but with some differences to help account for CSR effects. At the beginning of the lattice after the preparation of the bunch, the time and energy profiles are nearly identical but as the bunch travels through the accelerator, the profiles become distorted. Determining an initial distribution that would "use" CSR effects to its

[2] All bunch length measurements are the rms bunch length given by $\sigma_{z,rms} = \sqrt{< z^2 > - < z >^2}$ and all emittance values are the normalized, rms emittance given by $\epsilon_{rms,n} = \gamma\sqrt{< x^2 >< x'^2 > - < xx' >^2}$

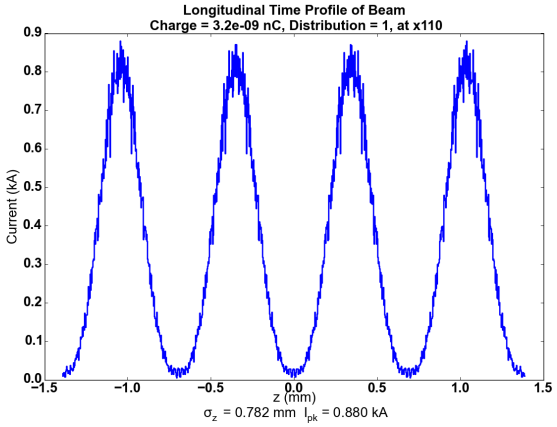

Figure 5: 1: Four peak Gaussians

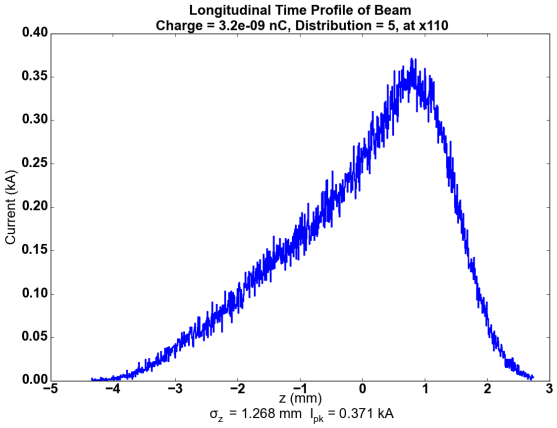

Figure 6: 5. Ramp

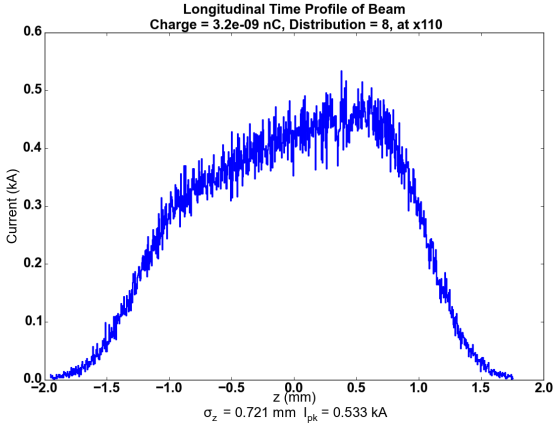

Figure 7: 8: Ideal-1

Table 1: Values for Summed Gaussian Functions

Distribution Number	Distribution Name	N	a_1	a_2	a_3	a_4	b_1	b_2	b_3	b_4
1	Four Peak Gaussians	4	1	1	1	1	0	6	12	18
5	Ramp	4	0.75	1.75	2.75	5	0	2	4	6
8	Ideal-1	4	2.5	2.7	2.95	3.75	0	1.85	3.5	5.3
9	Flat Top	4	1.1	1	1	1.1	0	1.95	3.85	5.8
10	Gaussian	1	1	-	-	-	0	-	-	-
12	Ideal-2	4	2.9	3.1	3.2	3.6	0	2	3.9	5.8
16	Ramp Backwards	4	0.75	1.75	2.75	5	0	-2	-4	-6
17	Ideal-2 Backwards	4	2.9	3.1	3.2	3.6	0	-2	-3.9	-5.8
18	Ideal-3	-	-	-	-	-	-	-	-	-

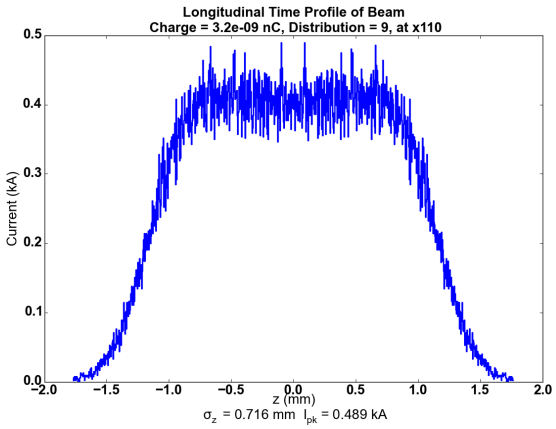

Figure 8: 9: Flat-Top

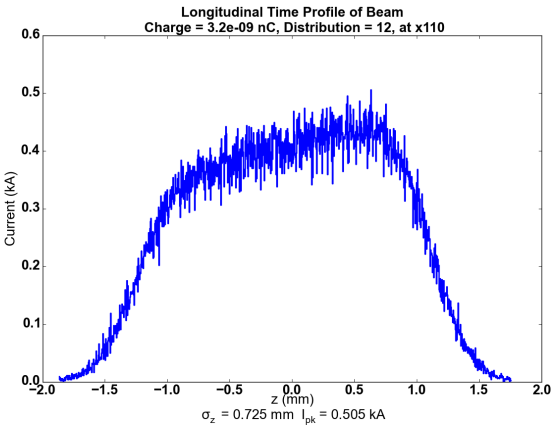

Figure 10: 12: Ideal-2

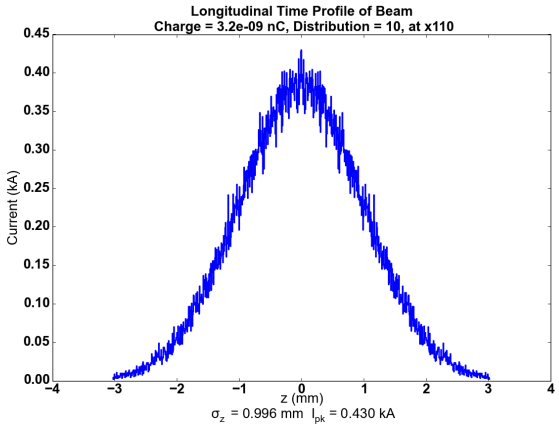

Figure 9: 10: Gaussian

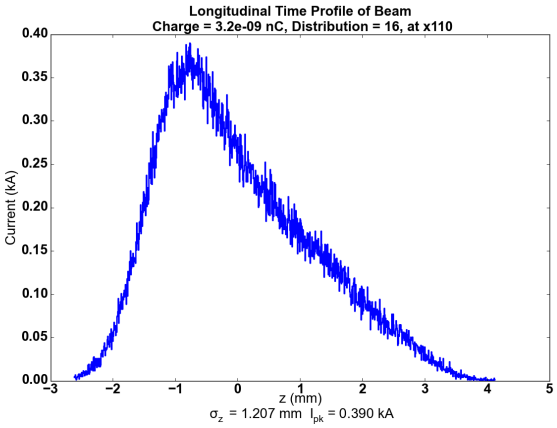

Figure 11: 16: Ramp Backwards

advantage to result in a flat energy profile is thus a form of an inverse problem in which we tried to back-engineer an initial time profile. A flat energy profile is desired because it allows for a uniform energy loss across the bunch.

To gain a better understanding of the effects of CSR on the energy profile of the bunch, simulations were run with CSR modeling in the dipole magnets and the drift spaces(this the standard for the rest of the paper unless otherwise specified) and in the dipoles only. Figure 14 shows the final energy profiles for each distribution using only CSR dipoles. At the default FWHM, many of the energy profiles come close to being flat with Dist. 12 being nearly flat but for the slight bend near the average energy. At a FWHM of 2.34 however, none of the distributions including number 18 come out flat. To determine the effects of simulating CSR in the drift spaces as well as the dipoles, Figure 15 is plotted showing the final energy profiles. From comparing Figure 14 and Figure 15, it becomes apparent

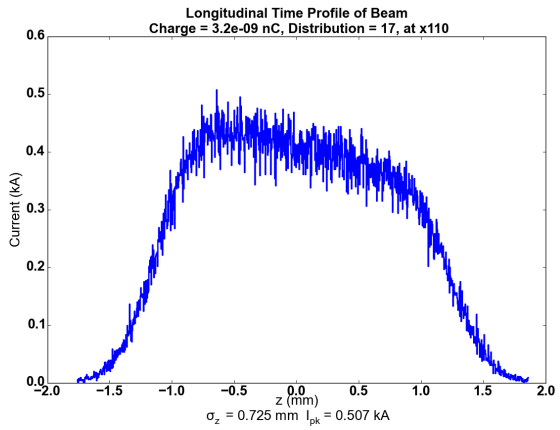

Figure 12: 17: Ideal-1 Backwards

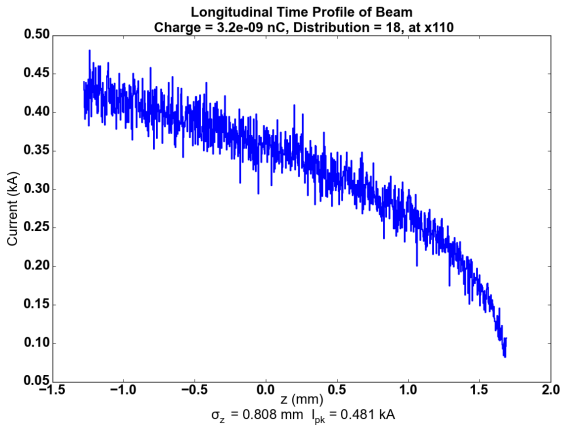

Figure 13: 18: Ideal-3

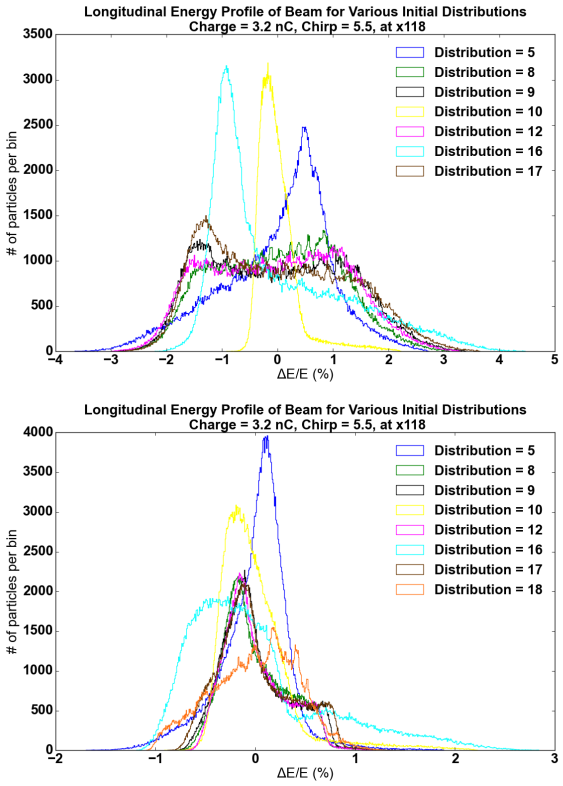

Figure 14: Energy Profile of the bunch plotted after the chicane with only CSR dipoles enabled. Top: FWHM = default Bottom: FWHM = 2.34 mm

that CSR in the drifts has, in general, a small effect on the longitudinal energy profile of the bunch. The bottom plot of 15 also indicates that once the noise is overlooked, the theoretical Dist. 18 has a nearly flat energy profile at the end of the lattice.

BRIGHTNESS RESULTS

1. FWHM Set to Default

In trying to decide on a suitable parameter to characterize the bunch length of distributions that could become greatly distorted as they propagated through the lattice, the full-width-half-max (FWHM) was chosen. We thought that it provided a consistent measure of the length of the bunch that could be used to compare one distribution to another. In hindsight we believe that using the rms normalized bunch length would have been a better and more consistent choice. It would have accounted more appropriately for the distortion effects that many of the profiles underwent in that it is statistically derived and does not contain in itself the implication that a strong, single peak exists like the FWHM does.

The crystal laser method of creating different initial charge distributions currently allows for the creation of multiple Gaussian distributions with a sigma (rms bunch length) of 3 ps (.9 mm) which can be combined to become any of the distributions simulated in this paper except number 18 which is more theoretical. The 'default' setting of the FWHM reflects this limitation. For this setting, each of the profiles is generated using a Gaussian function with a sigma of 1 mm. Each Gaussian is then combined with the offsets given in Table 1 in millimeters resulting in a varying overall FWHM max length that depends on the number of individual Gaussians and the length of the peak offsets. Table 3 shows a few of these.

The results of the run are shown in Figure 16. Upon first glance it might appear that the results indicate that many of the combined-Gaussian profiles result in lower horizontal emittance increases and in higher peak currents leading to greater peak brightness than the single Gaussian (here used almost like a control). In fact the emittance growth factor for the single gaussian remains around 2 times greater than that of the next highest distribution. This difference is due to the well documented phenomenon that the effects of CSR are greatly magnified at smaller bunch lengths [4]. This means that in our 'default' simulation, Dist 10 had much greater CSR effects acting on it than did any of the other profiles due to its smaller bunch length. Strictly comparing distributions here is therefore not very accurate be-

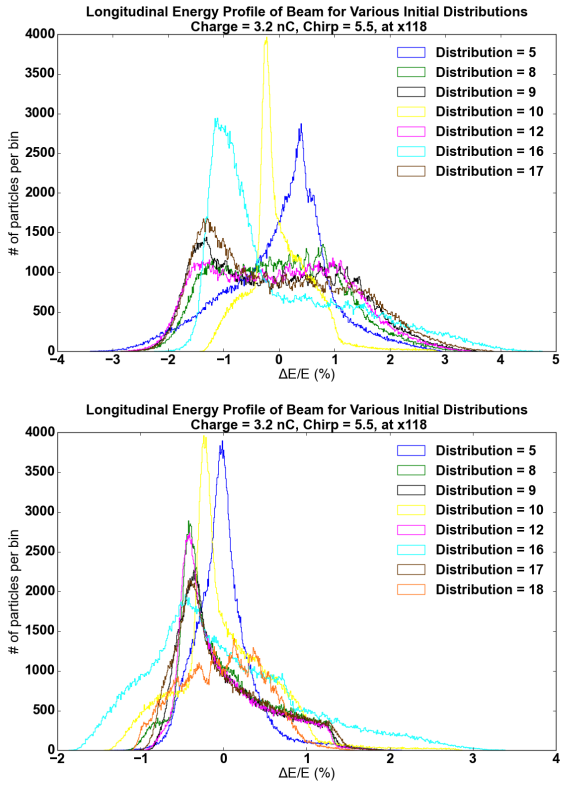

Figure 15: Energy Profile of the bunch plotted after the chicane with CSR dipoles and drifts enabled. Top: FWHM = default Bottom: FWHM = 2.34 mm

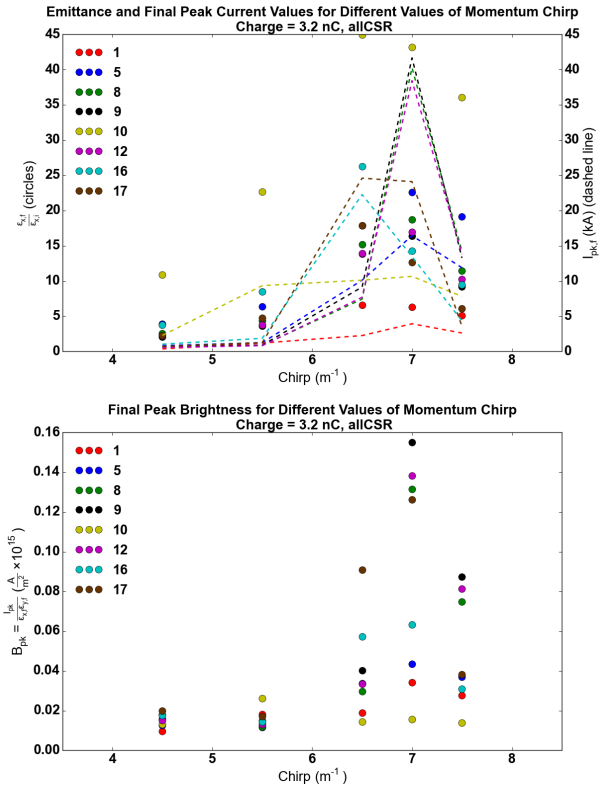

Figure 16: FWHM = default
Top; Emittance Growth Factor (circles) and Peak Current Values (dashed line) versus Chirp. Bottom; Peak Brightness versus Chirp

cause the emittance growth factor and final peak current differences recorded are as much products of the initial bunch length as they are of the shape of the initial charge distribution as will be seen conclusively in the next two sections.

Table 3: Bunch Length and FWHM Values Under 'default' Settings

Distribution Number	Initial σ_{rms} (mm)	Initial fwhm (mm)
1	6.787	20.3
10	1.001	2.34
12	2.385	7.7

FWHM Set to 2.34 mm

In addition to the simulations with the 'default' FWHM, two more runs were conducted with initial FWHM values of 2.34 mm and 7.7 mm. Our simulation indicates that it is not possible to simultaneously have a decreasing horizontal emittance growth and an increasing peak current as a function of different momentum chirps. Across nearly every distribution number and from any one chirp value to another, if the peak current increased, so did the emittance growth factor. The exceptions to this represent a general trend only in the case of Distribution 1 and in other singular cases, indicate what will turn out to be a favorable brightness value for a combination of distribution number and chirp. Because this is the case, the areas of interest become those in which the peak current increase is greater than that of the emittance growth factor and when the two are inversely related as just mentioned.

One of the first specific observations that must be made is that unlike in the 'default' case, the single Gaussian distribution (Dist. 10) does not have significantly greater values of emittance growth at all values of chirp. This leads to the conclusion that the difference by roughly a factor of 2 between the horizontal emittance growth of Dist. 10 and the distribution with the next highest value in the 'default' is indeed mostly due to the smaller bunch length of Dist. 10 as predicted.

At this fixed value of the initial FWHM length, our conclusion is that one single distribution does not provide the maximum brightness for all values of momentum chirp, but rather for given chirp value, there is a certain distribution that will allow for an optimized brightness. This being said there are some general trends that can be seen from looking at Figure 17. These are that Distributions 10 and 16 give consistently high values of peak current and that 16 and 5 give consistently lower values of emittance growth. Of the 'realistic' distributions (all but 18), the greatest brightness

is achieved by Dist. 5 for chirps of 4.5 and 7.5 m^{-1}, Dist. 16 for chirps of 5.5 and 6.5 m^{-1} and Dist. 17 for a chirp 7 m^{-1}. This being said, only at chirps of 4.5, 6.5 and 7.5 m^{-1} was there a significant increase over Dist. 10 as can be seen in Table 4 where the peak brightness values of Dist 10 are compared to the values of the distribution with the highest brightness. At higher values of chirp however, Dist. 18 has a peak brightness that is significantly better than any of the other distributions including Dist. 17 which is supposed to be its realistic copy. Glancing at the top plot of Figure 17 shows that this is because it's peak current increases by just over a factor of 5 from a chirp of 5.5 to 6.5 m^{-1} while its emittance growth increases by less than a factor of 1.25 over the same interval. That this theoretical distribution does so well is encouraging in that it helps to confirm Chad Mitchell's findings, but it still has very large values of emittance growth. 38374th5ygfnchcwu

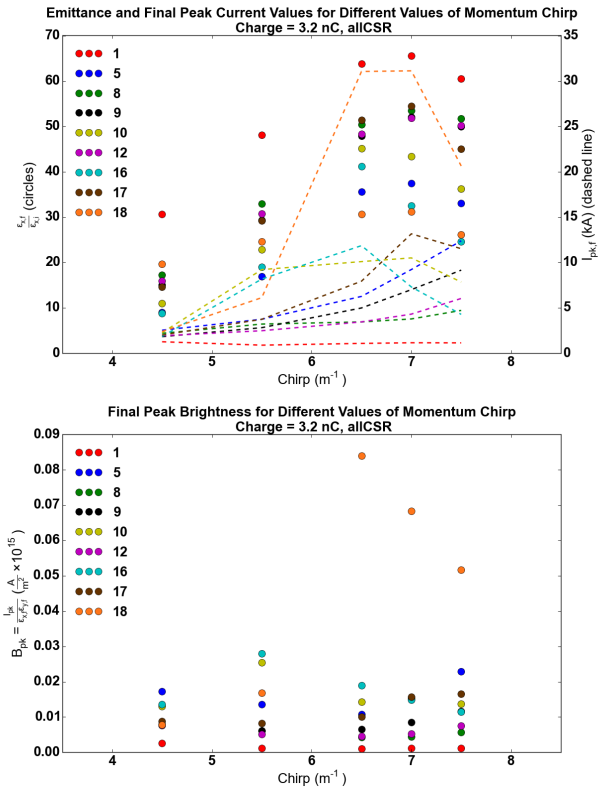

Figure 17: FWHM = 2.34 mm
Top; Emittance Growth Factor (circles) and Peak Current Values (dashed line) versus Chirp. Bottom; Peak Brightness versus Chirp

Table 4: Peak Brightness Comparison

Chirp	B_{pk} ($\frac{A}{m^2}$ × 1e15)(D10)	Greatest B_{pk} ($\frac{A}{m^2}$ × 1e15)	% Greater
4.5	0.013	0.0172	32.31
5.5	0.0255	0.0279	9.41
6.5	0.0143	0.019	32.87
7	0.0154	0.0157	1.95
7.5	0.0138	0.0229	65.94

FWHM Set to 2.34 mm with CSR Dipoles Only

Just as with the energy profiles, simulations were run without the CSR drifts "turned on" to determine the effect on the peak brightness. While this should in theory be less realistic than the case where both CSR drifts and CSR dipoles are used, it is useful to see how the effects are different using only one of these elements. The purposeful omission of the CSR drifts in most cases did not change the relationships between the distributions in terms of which ones had higher final peak brightness values, but did amplify the differences already present and increased the final brightness (seen in the bottom of Figure 18 for dipoles only and 17 for both).

To illustrate this take the example of a chirp of 5.5 m^{-1}. The peak brightness for all distributions had a percent increase of 101 ± 59.9 meaning that on average, each brightness value doubled from the CSR dipoles *and* drifts case to the CSR dipoles *only* case. While the overall values increased, the relative 'positions' of each distribution did not change much. Distributions 8, 9, 12, and 17 remained at the bottom with the lowest brightness values while distributions 5, 10, 16, and 18 remained at the top. Although they remained in much the same "order," the spacing between the brightness of the different distributions decreased when only the CSR dipoles were on. This is because the distributions at the bottom grew much more than the the distributions at the top which accounts for the high standard deviation in the mean increase. The maximum and minimum increase were by Dist 12 which had an increase of 182% and Dist. 10 which had an increase of only 15.9%. In general, the top distributions had a percent increase of 58.8 ± 61.3 (the high standard deviation being largely due to the increase of 146% of Dist. 5) while the bottom distributions had a percent increase of 144 ± 30.9.

It seems as though the CSR drifts serve to add to the effects of the CSR dipoles but not provide many different effects of their own (at least for the conditions of our simulation). The addition of the CSR drifts also serves to distinguish the brightness values of the different distributions from one another. Figure 18 shows that with only the CSR dipoles, the values of the brightness for most of the distributions are more tightly bunched than they are in Figure 17. Combined with the observations on the additive nature of the two sets effects, we predict that the longer CSR effects are present acting on the bunch, the greater the differences will be between different distributions.

FWHM Set to 7.7 mm

The final value of initial FWHM that was explored was 7.7 mm, so chosen because it was the the same FWHM that Dist. 12 had in the default setting. As was the case with the FWHM of 2.34 mm, Dist. 10 is does not have consistently higher values of emittance increase and smaller peak current like in the default case, further lending proof to the conclusion that the observations made in the default case were indeed due to the smaller initial FWHM (bunch

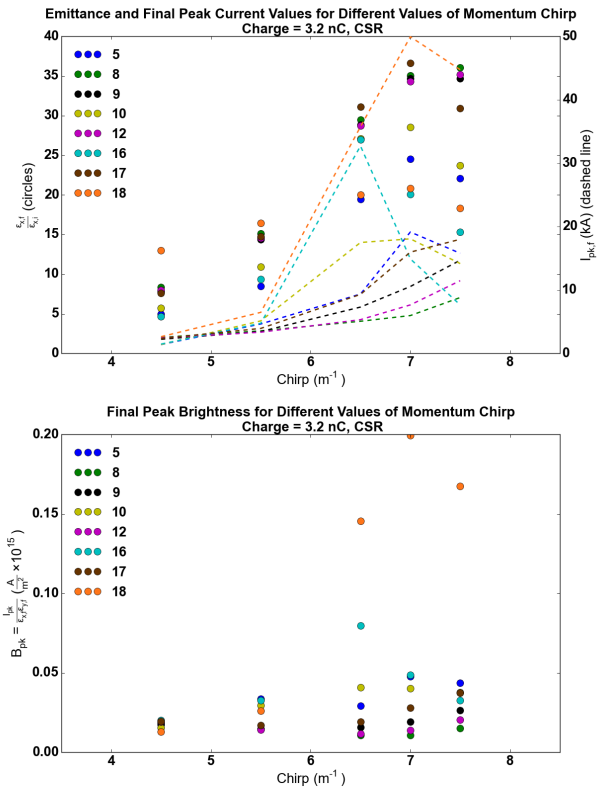

Figure 18: FWHM = 2.34 mm. CSR dipoles only
Top: Emittance Growth Factor (circles) and Peak Current Values (dashed line) versus Chirp. Bottom: Peak Brightness versus Chirp

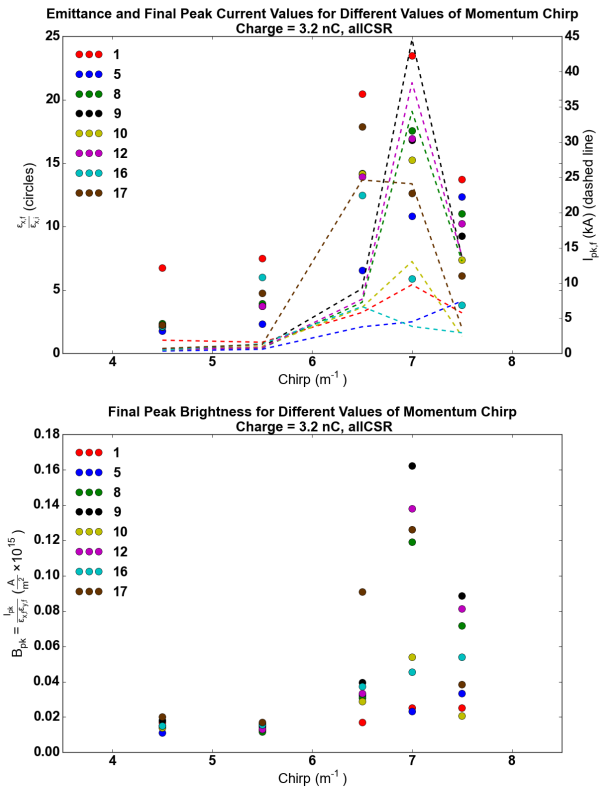

Figure 19: FWHM = 7.7 mm
Top; Emittance Growth Factor (circles) and Peak Current Values (dashed line) versus Chirp. Bottom; Peak Brightness versus Chirp

length). An interesting observation of this initial length compared to the FWHM of 2.34 mm is that for FWHM of 7.7 mm, every peak current curve has a very clear peak and begins to fall by a chirp of 7.5 m^{-1} except Dist. 5 while for FWHM of 2.34 mm, over half of the peak current curves are still rising by 7.5 m^{-1} (Figure 19). A future study incorporating many more chirp values to get smoother curves and an attempt to link this observation to the bunch compression itself would give insight into the effect of initial bunch length on the compression factor in realistic settings.

Peak Current Discussion

Note that defining the peak current as it is to be the maximum achievable current from the moving charge distribution has a limitation. For the data analysis presented in this paper, I calculated the peak current by finding the maximum of the charge density distribution (the maximum of the time profile)and then multiplying it by the speed the particles are traveling at, c. Because the charge density distribution is a histogram of the longitudinal position of each particle, there is an inherent dependence of the peak current on the bin size due to the statistical nature of the data. This effect should ideally be small though because built into my calculation is the relation $N_{\text{particles per bin}} \propto \frac{1}{N_{bins}}$ so the peak current should only fluctuate slightly given a changing bin size. I found that often this was not the case though with some profiles having peak currents that scaled proportionally with the number of bins. The reason for this is shown in Figure 20 which shows that many of the bins in the time array are empty for large a number of bins and that numbers fluctuate greatly even at a lower number of bins. For the bottom of Figure 20 the maximum is around 8 meaning there are fluctuations greater than half the max. Even with the number of bins as low as 50 and 25 (much too smaller to give good resolution), the peak current is dependent on the number of bins. This same phenomenon can be observed to a lesser degrees in many of the other time profiles once run through the lattice. See for example Figure 3 in which the time profile at watchstation x118 (after D4) has a large amount of noise. I do not know if this is a problem with the simulation code, my plotting code, or a meaningful physical statement but more inquiry into it would be justified and recommended. As it pertains to this paper, the absolute values of peak current and peak brightness do not have solid justification but the relative values which are under study are still valid.

```
>>> Current_kA[250:280]
array([  0.        ,   0.        ,   0.        ,  40.27657373,
         0.        ,   0.        ,   0.        ,   0.        ,
         0.        ,  39.11351377,   0.        ,   0.        ,
         0.        ,   0.        ,   0.        ,  39.63399917,
         0.        ,   0.        ,   0.        ,   0.        ,
         0.        ,  38.07254297,   0.        ,   0.        ,
         0.        ,   0.        ,   0.        ,  38.13037468,
         0.        ,   0.        ])
>>> Current_kA[20:40]
array([ 3.42042441,  7.31571142,  7.74238093,  3.97496626,  7.87603644
,
        7.93900875,  3.96339992,  7.62029177,  7.50655607,  3.60163044
,
        6.95586967,  6.60759425,  3.1756035 ,  6.15265146,  5.96823256
,
        2.94299151,  5.72341165,  5.71184531,  2.86973801,  5.59746704
```

Figure 20: Part of the array used to plot a bunch time profile. The same data is shown for two different values of number of bins. Top: 1000 bins. Bottom: 100 bins

THE SCRAPER

In an effort to simulate a practical method of achieving Dist 18, the $xscraper$ element was used in the dispersive section of the lattice between dipoles 2 and 3. The element simulates the usage of two pieces of metal foil that are positioned so as to block the passage of the particles at large and small values of x. This was done in the area between D2 and D3 because the final longitudinal position (z) of each particles is dependent on its x-position at this point. In fact, the correlation is such that "cutting" particles at the edge of the beam in x here will result in the loss of particles in the head and tail of the beam longitudinally at the end of the compressor. In this way we were hoping to be able to generate final time profiles with sharper edges and in particular, come closer to achieving Dist. 18 so as to minimize the horizontal emittance growth.

The method was not very successful though because the complicated way in which the energy and x-position of particles at the scraper location are related to the final longitudinal position meant the sharp edges we desire were not achievable. Much like how the creation of a large flat-walled pile of loose sand is difficult because the sand keeps falling and filling out the bottom of the pile, so too did the final time profiles always contain very similar head and tail effects to their non-scraped counterparts. Instead of achieving very sharp peaks, we only succeeded in sharpening the peaks a little and in moving the position of the head and/or tail in towards the center of the bunch.

CORE EMITTANCE

The motivation for looking into the core emittance of a bunch can be seen in Martin Reiser's statement, "The only problem with the rms emittance is that it gives more weight to the particles in the outer region of the trace-space [phase-space] area as compared to those in the beam core." [5] Determining the core emittance of the bunch will give a better understanding of how the majority of the particles in the bunch are behaving. In order to determine the core emittance, the $coreEmittance$ function in $ELEGANT$ was used. The $coreEmittance$ function slices the electron bunch into a portion of its former size and then calculates the emittance of this smaller bunch. In this case it is using 80%, 90%, and 100% of the beam to calculate the emittance values which are shown in Table 5. Reiser's statement is confirmed by our results as can be seen in Table 5. The table shows on average, a 20 to 40% emittance decrease for an 80% core of the beam corresponding to a decrease of up to 20% greater than the trivial level (a percent change of similar magnitude to the amount of the beam being cut).

For every value of chirp, nearly every other initial profile has a percent decrease in emittance that is greater then that of Dist. 10. In particular, Dist. 18 has the largest decrease of any of the distributions at the same values of chirp, 6.5, 7, and 7.5 m^{-1}, that it had the highest peak current value and nearly lowest emittance growth factor before.

SUMMARY

Preparing an initial current profile as a summation of Gaussian functions allows for an optimization of the horizontal emittance growth and peak current leading to a maximum brightness. Compared to the single Gaussian distribution though, the brightness increase of the other distributions was only significant for a few values of chirp and even then only by a factor less than 2 (for a fixed FWHM). When the FWHM values were allowed to differ based on the distribution, the final peak brightness of the idealized distributions was greater than that of the Gaussian but that was shown to be mostly due to the difference in initial bunch length and not the bunch shape. Distribution 18, although theoretical in nature, gives the highest values of final peak brightness at large values of chirp (near the point of maximum compression). With distribution 18, a nearly flat energy profile at the end of the bunch compressor is also possible. The final horizontal emittance numbers are very high but this is due to the high charge of 3.2 nC that we were running at. Simulation runs at a charge 250 pC resulted in emittance numbers between 1 and 5 μm and when only 90% of the beam was used, horizontal emittance growths of as low as 1-2%.

ACKNOWLEDGMENTS

I would sincerely like to thank everyone who made this wonderful summer of research possible. My mentor Charles Thangaraj has taught me an incredible amount this summer and helped guide me through my work from day one. I would also like to thank Eric Prebys and Tanja Waltrip for all their help making the Lee Tang internship happen and run smoothly and for their extra flexibility and effort in tweaking my work dates.

REFERENCES

[1] C. Mitchell, J. Qiang, and P. Emma, "Longitudinal pulse shaping for the suppression of coherent synchrotron

Table 5: Full and Partial Emittance Values with FWHM = 2.34 mm. Analysis for CSR dipoles only.

	Chirp (1/m)	**100%** $\epsilon_{x,f}$ (μm)	**90%** $\epsilon_{x,f}$ (μm)	% Change	**80%** $\epsilon_{x,f}$ (μm)	% Change
5	4.5	20.02	15.83	-20.9291	13.473	-32.7023
8	4.5	33.671	25.244	-25.0275	20.047	-40.4621
9	4.5	31.185	21.148	-32.1853	15.457	-50.4345
10	4.5	22.949	17.551	-23.5217	14.036	-38.8383
12	4.5	32.027	23.28	-27.3113	17.976	-43.8724
16	4.5	18.482	12.417	-32.8157	9.163	-50.422
17	4.5	30.366	19.56	-35.5859	13.378	-55.9441
18	4.5	53.244	36.799	-30.8861	27.079	-49.1417
5	5.5	34.297	27.289	-20.4333	23.369	-31.8628
8	5.5	60.944	46.709	-23.3575	37.179	-38.9948
9	5.5	57.755	41.795	-27.634	31.158	-46.0514
10	5.5	43.667	33.36	-23.6036	26.695	-38.8669
12	5.5	58.592	44.175	-24.6057	34.367	-41.3452
16	5.5	36.936	26.261	-28.9013	20.099	-45.5843
17	5.5	58.67	41.207	-29.7648	29.766	-49.2654
18	5.5	67.483	50.016	-25.8836	38.946	-42.2877
5	6.5	79.24	67.256	-15.1237	56.855	-28.2496
8	6.5	118.812	98.042	-17.4814	81.681	-31.2519
9	6.5	116.102	91.697	-21.0203	74.332	-35.977
10	6.5	108.456	94.286	-13.0652	86.698	-20.0616
12	6.5	115.596	94.255	-18.4617	77.429	-33.0176
16	6.5	106.319	94.604	-11.0187	88.275	-16.9716
17	6.5	123.735	95.331	-22.9555	81.287	-34.3056
18	6.5	81.922	62.708	-23.454	52.349	-36.099
5	7	99.852	88.089	-11.7804	76.497	-23.3896
8	7	141.27	122.007	-13.6356	104.526	-26.0098
9	7	139.72	117.191	-16.1244	100.067	-28.3803
10	7	114.232	103.309	-9.56212	95.15	-16.7046
12	7	138.286	118.633	-14.2119	101.353	-26.7077
16	7	79.078	68.055	-13.9394	62.15	-21.4067
17	7	145.735	122.217	-16.1375	110.826	-23.9538
18	7	85.522	66.619	-22.1031	59.39	-30.5559
5	7.5	89.958	77.549	-13.7942	66.127	-26.4913
8	7.5	145.393	127.551	-12.2716	113.22	-22.1283
9	7.5	139.759	121.961	-12.7348	109.131	-21.9149
10	7.5	94.864	81.973	-13.5889	74.149	-21.8365
12	7.5	141.741	124.517	-12.1517	110.976	-21.7051
16	7.5	60.1	50.847	-15.396	45.753	-23.8719
17	7.5	122.901	99.587	-18.9697	88.573	-27.9314
18	7.5	75.233	55.585	-26.1162	50	-33.5398

radiation-induced emittance growth," *Phys. Rev. ST Accel. Beams*, vol. 16, p. 060703, Jun 2013.

[2] M. Borland, "elegant: A flexible sdds-compliant code for accelerator simulation," *Advanced Photon Source LS-287*, 2000.

[3] J. G. Power and C. Jing, "Temporal laser pulse shaping for RF photocathode guns: The cheap and easy way using UV birefringent crystals," *AIP Conf.Proc.*, vol. 1086, pp. 689–694, 2009.

[4] J. C. T. Thangaraj, R. Thurman-Keup, J. Ruan, A. S. Johnson, A. H. Lumpkin, and J. Santucci, "Experimental studies on coherent synchrotron radiation at an emittance exchange beam line," *Phys. Rev. ST Accel. Beams*, vol. 15, p. 110702, Nov 2012.

[5] M. Reiser, *Theory and design of charged particle beams*. John Wiley & Sons, 2008.